



# Two-Dimensional Conjugated Metal-Organic Frameworks with Large Pore Apertures and High Surface Areas for NO<sub>2</sub> Selective Chemiresistive Sensing

Pei Chen, Xi Su, Chuanzhe Wang, Guang Zhang, Ting Zhang, Gang Xu,\* and Long Chen\*

**Abstract:** The emergence of two-dimensional conjugated metal-organic frameworks (2D *c*-MOFs) with pronounced electrical properties (e.g., high conductivity) has provided a novel platform for efficient energy storage, sensing, and electrocatalysis. Nevertheless, the limited availability of suitable ligands restricts the number of available types of 2D *c*-MOFs, especially those with large pore apertures and high surface areas are rare. Herein, we develop two new 2D *c*-MOFs (HIOTP-*M*, *M*=Ni, Cu) employing a large *p*- $\pi$  conjugated ligand of hexaamino-triphenylene[2,3-*b*:6,7-*b'*:10,11-*b''*]tris[1,4]benzodioxin (HAOTP). Among the reported 2D *c*-MOFs, HIOTP-Ni exhibits the largest pore aperture of 3.3 nm and one of the highest surface areas (up to 1300 m<sup>2</sup>g<sup>-1</sup>). As an exemplary application, HIOTP-Ni has been used as a chemiresistive sensing material and displays high selective response (405 %) and a rapid response (1.69 min) towards 10 ppm NO<sub>2</sub> gas. This work demonstrates significant correlation linking the pore aperture of 2D *c*-MOFs to their sensing performance.

**M**etal-organic frameworks (MOFs), a flourishing family of crystalline porous materials, are assembled via the coordination between metal ions/clusters and organic ligands.<sup>[1]</sup> Due to their tunable structures and permanent porosity, MOFs

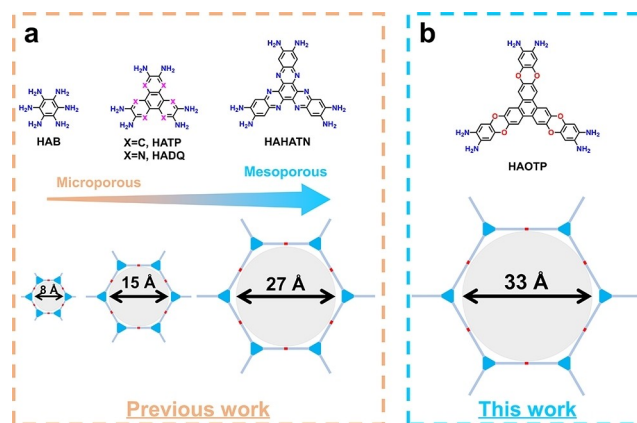
have shown immense potential for various applications such as catalysis,<sup>[2]</sup> biosensing,<sup>[3]</sup> gas storage and separation.<sup>[4]</sup> However, their insulating property results in moderate performance for electrochemical applications.<sup>[5]</sup> Two-dimensional conjugated MOFs (2D *c*-MOFs) possess high electrical conductivities due to the extended in-plane  $d$ - $\pi$  conjugation among the metal ions and ligands, generating graphene-like structures while inheriting the permanent porosities of traditional MOFs.<sup>[6]</sup> These materials with high intrinsic charge mobility deliver more opportunities for energy storage, electrocatalysis, chemiresistive sensing, etc.<sup>[7]</sup> Despite their promising achievements, the types of 2D *c*-MOFs are currently limited by the availability of suitable ligands. Generally, the organic ligands for 2D *c*-MOFs are mainly comprised of C<sub>3</sub>-,<sup>[8]</sup> C<sub>4</sub>-,<sup>[9]</sup> and C<sub>6</sub>-symmetric<sup>[10]</sup> units containing *ortho*-substituted coordination sites (OH, NH<sub>2</sub>, SH), and their sizes greatly influence the pore apertures of 2D *c*-MOFs. For example, with the ligand size increasing from HAB,<sup>[8h]</sup> to HATP<sup>[8d]</sup> and HAHATN,<sup>[8c]</sup> the corresponding 2D *c*-MOFs showcase aperture sizes of 8 Å, 15 Å and 27 Å, respectively. (Scheme 1a). Nonetheless, most of ligands were produced through formulaic synthetic methods, such as HATP<sup>[8d]</sup> and HATI<sup>[8i]</sup> were synthesized via Buchwald–Hartwig coupling reactions and following by hydrolysis reactions, and thus may not be atom-economical. Therefore, developing new organic ligands with alternative synthetic procedures is highly desirable and challenging.

[\*] P. Chen, X. Su, Dr. G. Zhang, Prof. L. Chen  
Department of Chemistry, Tianjin Key Laboratory of Molecular Optoelectronic Science, Tianjin University  
Tianjin 300072 (China)  
E-mail: long.chen@tju.edu.cn

C. Wang, Prof. G. Xu  
Fujian Science & Technology Innovation Laboratory for Optoelectronic Information of China Fuzhou  
Fujian 350108 (China)  
E-mail: gxu@fjirsm.ac.cn

Dr. T. Zhang  
College of Chemistry and Chemical Engineering, Liaoning Normal University  
Dalian 116029 (China)

Prof. L. Chen  
State Key Laboratory of Supramolecular Structure and Materials, College of Chemistry, Jilin University  
Changchun 130012 (China)  
E-mail: longchen@jlu.edu.cn



**Scheme 1.** a) The reported C<sub>3</sub>-symmetric organic ligands with amino groups and pore sizes of the corresponding 2D *c*-MOFs. b) Our new C<sub>3</sub>-symmetric organic ligand with extended *p*- $\pi$  conjugation and the large pore apertures of HIOTP-*M*.

Recently, 2D *c*-MOFs have been employed in chemiresistive sensing due to their extraordinary properties that can enhance the surface reactions and adsorptions of gas molecules.<sup>[11]</sup> In contrast to carbon-based nanomaterials,<sup>[12]</sup> hybrid materials,<sup>[13]</sup> and semiconducting metal oxides,<sup>[14]</sup> 2D *c*-MOF-based chemiresistive sensors exhibit high selectivity and can operate at room temperature. Normally, the detection process of chemiresistive sensors relies on the transduction of surface reactions into electrical signals i.e. resistances, conductance.<sup>[15]</sup> However, 2D *c*-MOFs always show moderate response values and long response time due to their relatively few accessible active sites and low mass transport efficiency, which is highly influenced by the pore size, surface area, particle size and morphology of materials.<sup>[16]</sup> Therefore, developing 2D *c*-MOFs with suitable pore apertures, high surface areas, and robust adaptability is essential for practical applications in chemiresistive sensing.

Herein, we designed and newly synthesized hexaamino-triphenyleno[2,3-*b*:6,7-*b'*:10,11-*b''*]tris[1,4]-benzodioxin (HAOTP), a larger extended organic ligand through nucleophilic substitution and nitro-reduction reactions, to fabricate two new 2D *c*-MOFs (HIOTP-*M*, *M*=Ni, Cu). To the best of our knowledge, HIOTP-Ni represents one of the highest surface areas (up to 1300 m<sup>2</sup> g<sup>-1</sup>) and the largest pore apertures (3.3 nm) among reported 2D *c*-MOFs (Scheme 1b, Figure 2). ■■■ Dear author please mention Figure 1 ahead

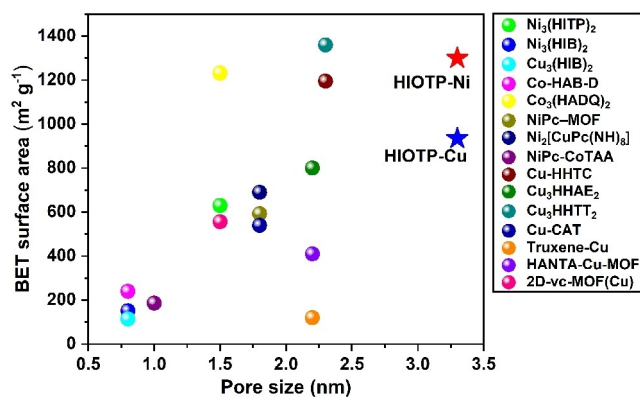


**Figure 2.** The plot of BET surface area against pore size in reported of some typical 2D *c*-MOFs.

Figure 2 ■■■ Significantly, the HIOTP-Ni-based chemiresistive sensor displayed high sensitivity, selectivity, and rapid response toward 10 ppm NO<sub>2</sub>. Based on the comparisons, we conclude that both the pore aperture impact the sensor performance.

HAOTP was unambiguously characterized by solution nuclear magnetic resonance (NMR) spectroscopy and high resolution mass spectrometry (HR-MS, Figures S1, S2, and

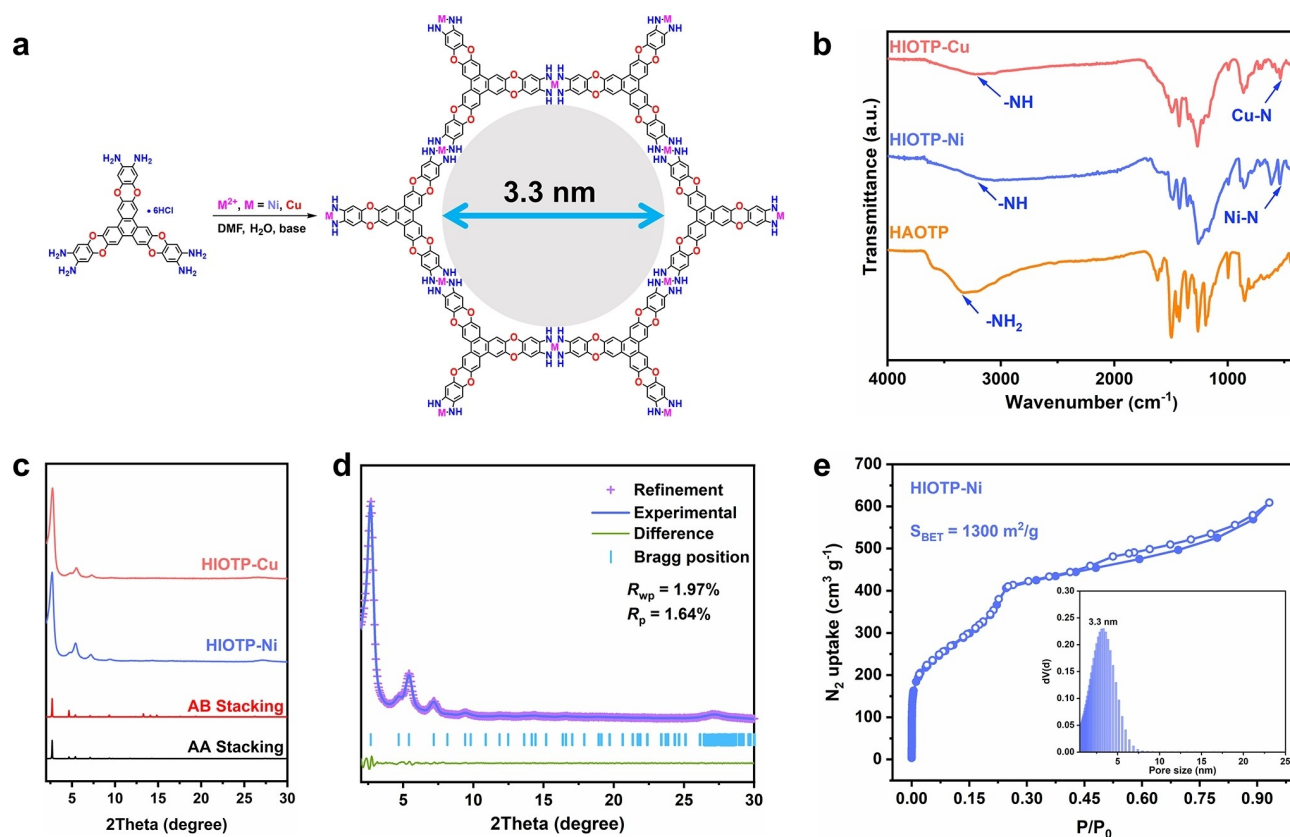


**Figure 1.** a) Schematic representation of the synthesis procedure and structure. b) FT-IR spectra of HAOTP, HIOTP-Ni, and HIOTP-Cu. c) Simulated and experimental PXRD patterns for HIOTP-*M*. d) Experimental and Pawley fitted PXRD patterns of HIOTP-Ni. e) N<sub>2</sub> sorption isotherm of HIOTP-Ni at 77 K (inset: pore width distribution).

S3). The stable hydrochloride salt of HAOTP was reacted with metal nitrates under basic conditions to produce HIOTP-*M* (Figure 1a, see Supporting Information for synthetic details). HIOTP-*M* were characterized by Fourier transform infrared (FT-IR) spectroscopy (Figure 1b). The broad signal at  $3240\text{ cm}^{-1}$  was attributed to N–H stretching vibrations of the amino groups from the ligand HAOTP, while the signal at  $536\text{ cm}^{-1}$  was attributed to the coordination bond between the amino nitrogen and metal ions,<sup>[17]</sup> confirming the successful coordination between HAOTP and metal ions.

The crystalline structures of HIOTP-*M* were characterized by powder X-ray diffraction (PXRD) analysis. The PXRD patterns of both MOFs were almost identical, exhibiting strong diffraction peaks at  $2.70^\circ$ ,  $4.65^\circ$ ,  $5.40^\circ$  and  $27.20^\circ$ , which could be assigned to the (100), (110), (200), and (001) facets, respectively. Both AA and AB stacking models were constructed using Materials Studio software to reveal the packing structures of the as-prepared MOFs (Figures S4 and S5). The simulated PXRD patterns of the AA-stacking frameworks fitted better with the experimental ones (Figure 1c). Pawley refinement provided the cell parameters of HIOTP-Ni as follows:  $a=b=37.90\text{ \AA}$ ,  $c=3.28\text{ \AA}$ ,  $\alpha=\beta=90^\circ$ ,  $\gamma=120^\circ$  in *P6/MMM* space group, with small  $R_{\text{wp}}$  and  $R_p$  of 1.97% and 1.64%, respectively (Figure 1d). Similarly, the unit cell parameters of HIOTP-Cu were:  $a=b=38.17\text{ \AA}$ ,  $c=3.34\text{ \AA}$ ,  $\alpha=\beta=90^\circ$ ,  $\gamma=120^\circ$  in *P6/MMM* space group, with reasonable  $R_{\text{wp}}$  and  $R_p$  of 3.11% and 2.50%, respectively (Figure S6).

The permanent porosities of HIOTP-*M* were estimated by nitrogen sorption measurements at 77 K. The sorption isotherms of both HIOTP-Ni and HIOTP-Cu exhibited typical type-IV characteristics (Figure 1e and Figure S7). Remarkably, the Brunauer–Emmett–Teller (BET) surface areas of HIOTP-Ni and HIOTP-Cu were calculated to be 1300 and  $935\text{ m}^2\text{ g}^{-1}$ , respectively (Figure S8). HIOTP-Ni exhibited a narrow pore size distribution centered at 3.3 nm as calculated by nonlocal density functional theory (NLDFT), consistent with the theoretical value (3.3 nm) based on the AA-stacking model (Figure 1e). As a comparison, we summarized the BET surface areas and pore sizes of some representative 2D *c*-MOFs reported before (Figure 2 and Table S1). Notably, HIOTP-*M* possess the largest pore apertures among the reported 2D *c*-MOFs, and the BET surface area of HIOTP-Ni is higher than that of most reported 2D *c*-MOFs, except for  $\text{Cu}_3\text{HHTT}_2$  reported by Dincă and co-workers.<sup>[8b]</sup>

The thermal stabilities of HIOTP-*M* were evaluated by thermogravimetric analysis (TGA, Figures S9 and S10). HIOTP-Ni and HIOTP-Cu retained 90% of their initial mass up to 314 and  $198^\circ\text{C}$ , respectively. The morphologies of HIOTP-*M* were characterized using scanning electron microscopy (SEM) and transmission electron microscopy (TEM, Figures S11, S12, S13, and S14). The clear lattice fringes in high-resolution TEM image further proved the crystalline feature of HIOTP-Ni (Figure S12b). X-ray photoelectron spectroscopy (XPS) analysis of HIOTP-*M* revealed the presence of C, N, O, and metal ions (Figures S15 and S17). The high-resolution spectra of C 1s, O 1s, and N 1s for

both MOFs exhibited similar characteristics (Figures S16 and S18). Moreover, both the XPS spectra of N 1s showcased only one type of N existed in the frameworks, indicating that HIOTP-*M* were neutral and no cationic or anionic ions ( $\text{NH}_4^+$ ,  $\text{Cl}^-$ ) were present. The XPS spectrum of Ni 2p for HIOTP-Ni exhibited a dominant peak belonging to  $\text{Ni}^{2+}$  at approximately 855.8 eV. The XPS spectrum of Cu 2p for HIOTP-Cu displayed two distinct peaks at about 935.1 and 932.9 eV, indicating the co-existence of both  $\text{Cu}^{2+}$  and  $\text{Cu}^+$ .

The ultraviolet-visible-near infrared (UV/Vis-NIR) spectra of HIOTP-Ni and HIOTP-Cu exhibited notable absorption at 1087 and 1056 nm, respectively (Figures S20a and S21a). The band gaps of HIOTP-Ni and HIOTP-Cu were calculated to be 1.16 and 1.40 eV, respectively, using the Tauc plot method (Figures S20b and S21b). The ultraviolet photoelectron spectroscopy (UPS) results revealed that the HOMO of HIOTP-Ni and HIOTP-Cu was  $-5.25$  and  $-5.91$  eV, respectively, indicating that HIOTP-Ni is more prone to losing electrons (Figure S19, Table S2). The electrical conductivities of HIOTP-*M* were measured under ambient conditions through the two-point probe method on a pressed pellet. HIOTP-Ni and HIOTP-Cu exhibited modest electrical conductivities of  $4.07\times 10^{-6}$  and  $4.75\times 10^{-7}\text{ S m}^{-1}$ , respectively (Figures S22 and S23). To further confirm the charge transport ability of HIOTP-*M*, an iodine doping experiment was performed. Iodine-doped HIOTP-Ni and iodine-doped HIOTP-Cu displayed an enhancement in electrical conductivities to  $8.0\times 10^{-4}$  and  $6.7\times 10^{-4}\text{ S m}^{-1}$ , respectively (Figures S24 and S25). Furthermore, variable-temperature conductivity measurements from 273 to 313 K revealed the thermally-activated charge transport capability of HIOTP-*M*, indicating their typical semiconducting behavior (Figures S26–S29).

Benefiting from their large pore apertures, high surface areas, and potential mass transport efficiency, HIOTP-*M* were used for chemiresistive sensing and tested in a home-made sensing system.<sup>[18]</sup> We initially investigated the response of HIOTP-*M*-based chemiresistive sensors to different gases and volatile organic compounds (VOCs) at a concentration of 100 ppm. Remarkably, HIOTP-Ni showed a much higher response to nitrogen dioxide ( $\text{NO}_2$ ) gas than other test gases, indicating its excellent selectivity towards  $\text{NO}_2$  gas (Figure 3a). In contrast, HIOTP-Cu displayed no significant responses to any test gas, despite its superior response to  $\text{NO}_2$  gas compared to other gases (Figures S30 and S31).

We evaluated the sensitivity of HIOTP-Ni towards  $\text{NO}_2$  across the concentration range of 1–100 ppm, and the obtained current curve demonstrated good response-recovery performance (Figure 3b). Following this, we conducted five consecutive response-recycle processes of HIOTP-Ni under 10 ppm  $\text{NO}_2$ , which revealed only 1.3% of the coefficient of variation (CV), thereby confirming the good response repeatability (Figure 3c). The average response of HIOTP-Ni towards 10 ppm  $\text{NO}_2$  was calculated to be 405%. Furthermore, the log-log plots of response-concentration of HIOTP-Ni towards  $\text{NO}_2$  showcased good linearity ( $R^2=0.98$ ) within the range of 1–100 ppm.

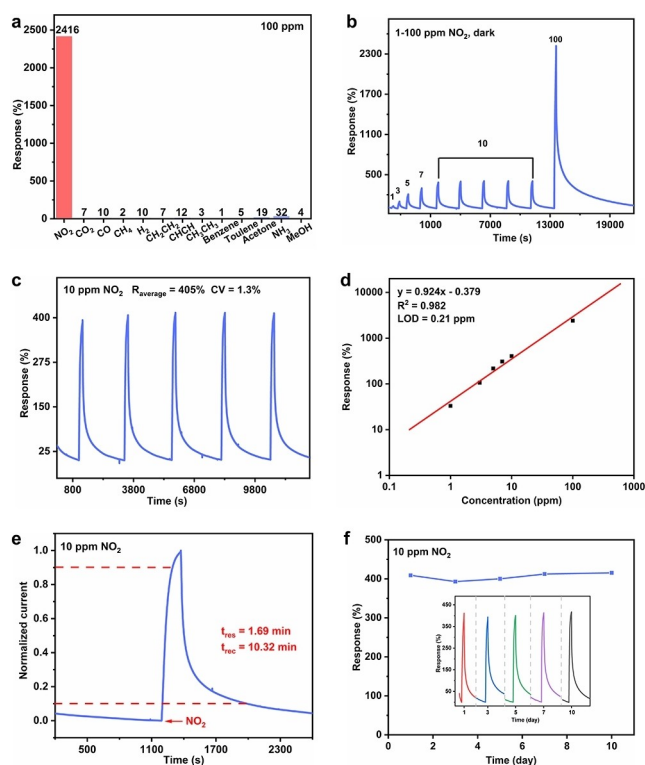


**Figure 3.** Gas-sensing performances of the devices at room temperature. a) Response ability toward different gas of HIOTP-Ni (b) Dynamic response curves of HIOTP-Ni toward 1–100 ppm NO<sub>2</sub>. c) Response-recycle toward 10 ppm NO<sub>2</sub> of HIOTP-Ni. d) Linear relationship of response vs. NO<sub>2</sub> concentration of HIOTP-Ni. e) Normalized response-recovery time curves for HIOTP-Ni to 10 ppm NO<sub>2</sub>. f) Stability of HIOTP-Ni to 100 ppm NO<sub>2</sub> within 10 days.

Additionally, the theoretical limit of detection (LOD) was calculated to be 0.21 ppm (Figure 3d), which was lower than that of all 2D *c*-MOF powders and their composite materials (Tables S3 and S4).

We further evaluated the response time ( $t_{res}$ , the time required for increasing the current to 90% of the maximum value) and recovery time ( $t_{rec}$ , the time required for decreasing the maximum current value to its 10%) of HIOTP-Ni upon exposure to 10 ppm NO<sub>2</sub> and dry synthetic air, respectively (Figure 3e). The calculated values of  $t_{res}$  and  $t_{rec}$  for HIOTP-Ni were 1.69 and 10.32 min, respectively. To make a direct comparison, we synthesized two well-known 2D *c*-MOFs Ni<sub>3</sub>(HIB)<sub>2</sub> and Ni<sub>3</sub>(HITP)<sub>2</sub> which were reported to have smaller pore apertures and lower surface areas compared to HIOTP-Ni (Figure S32). We tested their sensing performance such as the response value,  $t_{res}$ , and  $t_{rec}$  towards 100 ppm NO<sub>2</sub> (Figures S33 and S34). We found that Ni<sub>3</sub>(HIB)<sub>2</sub> and Ni<sub>3</sub>(HITP)<sub>2</sub> showcased lower response of 138% and 71%, respectively, longer response time of 2.73 and 2.25 min, respectively, and the both disability of recovery at room temperature. Based on the experimental NO<sub>2</sub> sensing results of these 2D *c*-MOFs, as well as their large pore structures and high surface areas, we speculate that the diffusion rate of NO<sub>2</sub> inside the material, i.e., the

mass transport efficiency, plays an important role in NO<sub>2</sub> sensing.

Furthermore, we compared with other MOFs-based chemiresistive sensors, which tested at room temperature in the dark without heating or illumination. The response value and response time of HIOTP-Ni were superior than that of all 2D *c*-MOF powders and some other MOF composite materials, respectively (Tables S3 and S4). No obvious changes in response were observed after 10 days, demonstrating that HIOTP-Ni holds a good long-term stability (Figure 3f). In addition, PXRD and N<sub>2</sub> sorption measurements exhibited the preserved crystal structure and porosity of HIOTP-Ni, respectively, indicating its high stability after the NO<sub>2</sub> sensing test (Figures S35 and S36).

To gain further insights into the high selective sensing performance of HIOTP-Ni towards NO<sub>2</sub>, DFT calculations were conducted. The adsorption energy ( $E_{ad}$ ) between the Ni center of HIOTP-Ni and four different gas molecules (e.g., NO<sub>2</sub>, ammonia (NH<sub>3</sub>), carbon dioxide (CO<sub>2</sub>), and acetone) were computed (Figure S37 and Table S5). The simulated results indicated that the Ni center of HIOTP-Ni had the largest  $E_{ad}$  of  $-0.590$  eV to NO<sub>2</sub> among all gas molecules, supporting the high selectivity of HIOTP-Ni towards NO<sub>2</sub>. Similarly, the  $E_{ad}$  between the Cu metal sites of HIOTP-Cu and NO<sub>2</sub> was calculated (Figure S38 and Table S6). Apart from its higher surface area and electrical conductivity, the slightly larger adsorption energy of HIOTP-Ni toward NO<sub>2</sub> may also contribute to its better response ability in comparison with HIOTP-Cu.

The adsorption of NO<sub>2</sub> on HIOTP-Ni was further confirmed by XPS analysis. Upon exposure of HIOTP-Ni to NO<sub>2</sub>, a new peak of N 1s was observed at the binding energy of 406.7 eV (Figure 4a), indicating the coordination of NO<sub>2</sub> molecules to the Ni center, and the peak of Ni 2p also changed (Figure 4b and Figure S39).<sup>[19]</sup> Based on the DFT calculations, XPS, and experimental results, a possible NO<sub>2</sub> sensing process of HIOTP-Ni was proposed (Figure 4c): HIOTP-Ni-based chemiresistive sensor can rapidly adsorb NO<sub>2</sub> and donate electrons, leading to an increase of hole

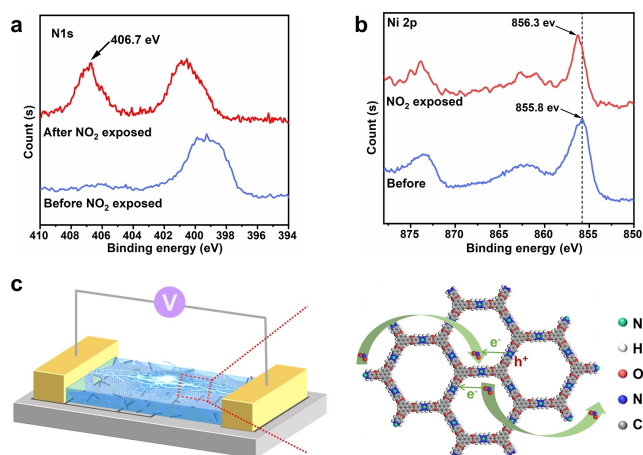


**Figure 4.** XPS spectra of a) N 1s b) Ni 2p range of HIOTP-Ni before and after NO<sub>2</sub> exposure. c) the gas sensor and the possible sensing process of HIOTP-Ni for NO<sub>2</sub>.

concentration in HIOTP-Ni and a subsequent change in electrical conductivity.<sup>[20]</sup> Consequently, upon NO<sub>2</sub> removal from HIOTP-Ni, the trapped electrons can be released back to the framework, leading to the current recovery of the sensor.

In summary, we have successfully developed two novel 2D *c*-MOFs (HIOTP-*M*, *M*=Ni, Cu) based on an elaborately designed ligand (HAOTP) with extended conjugation. Among reported 2D *c*-MOFs, HIOTP-Ni exhibits one of the highest surface areas (up to 1300 m<sup>2</sup> g<sup>-1</sup>) and the largest pore apertures of 3.3 nm. Owing to its porosity and electrical conductivity, the HIOTP-Ni-based chemiresistive sensor showcases high selective response (405 %) toward 10 ppm NO<sub>2</sub> gas, a rapid response (1.69 min), and mild recovery conditions, indicating its robust adaptability to the practical operating environment for NO<sub>2</sub> detection. The current work not only stimulates the development of novel 2D *c*-MOFs with larger pore apertures and higher surface areas but also provides new insights into applying 2D *c*-MOFs in diverse electronic devices. Furthermore, due to their increased active surface area and highly exposed active sites, 2D *c*-MOFs thin films show good performance in gas sensing.<sup>[11]</sup> Therefore, we are currently focusing on developing high-quality HIOTP-Ni MOF thin films toward better sensing devices.

### Acknowledgements

This work was financially supported by National Natural Science Foundation of China (51973153, 22171263) and National Key Research and Development Program of China (2017YFA0207500). Scientific Research and Equipment Development Project of CAS (YJKYQ20210024), Fujian Science & Technology Innovation Laboratory for Optoelectronic Information of China (2021ZR101) and the Natural Science Foundation of Fujian Province (2021J02017).

### Conflict of Interest

The authors declare no conflict of interest.

### Data Availability Statement

The data that support the findings of this study are available in the Supporting Information of this article.

**Keywords:** Electrical Conductivity · Electrical Device · Gas Sensing · Large Pore Apertures · Metal-Organic Frameworks

- [1] G. Cai, P. Yan, L. Zhang, H. Zhou, H. Jiang, *Chem. Rev.* **2021**, *121*, 12278–12326.  
 [2] a) Y. Huang, J. Liang, X. Wang, R. Cao, *Chem. Soc. Rev.* **2017**, *46*, 126–157; b) Y. Wei, M. Zhang, R. Zou, Q. Xu, *Chem. Rev.* **2020**, *120*, 12089–12174; c) J. Du, F. Li, L. Sun, *Chem. Soc. Rev.* **2021**, *50*, 2663–2695.

- [3] a) X. Liao, H. Fu, T. Yan, J. Lei, *Biosens. Bioelectron.* **2019**, *146*, 111743; b) Y. Zhao, H. Zeng, X. Zhu, W. Lu, D. Li, *Chem. Soc. Rev.* **2021**, *50*, 4484–4513.  
 [4] a) R. Lin, S. Xiang, W. Zhou, B. Chen, *Chem* **2020**, *6*, 337–363; b) W. Fan, X. Zhang, Z. Kang, X. Liu, D. Sun, *Coord. Chem. Rev.* **2021**, *443*, 213968.  
 [5] a) W. T. Koo, J. S. Jang, I. D. Kim, *Chem* **2019**, *5*, 1938–1963; b) M. Yao, W. Li, G. Xu, *Coord. Chem. Rev.* **2021**, *426*, 213479.  
 [6] a) L. Xie, G. Skorupskii, M. Dinca, *Chem. Rev.* **2020**, *120*, 8536–8580; b) M. Wang, R. Dong, X. Feng, *Chem. Soc. Rev.* **2021**, *50*, 2764–2793.  
 [7] a) G. Zhang, L. Jin, R. Zhang, Y. Bai, R. Zhu, H. Pang, *Coord. Chem. Rev.* **2021**, *439*, 213915; b) Y. M. Jo, Y. K. Jo, J. H. Lee, H. W. Jang, I. S. Hwang, D. J. Yoo, *Adv. Mater.* **2023**, *35*, 2206842.  
 [8] a) X. Song, X. Wang, Y. Li, C. Zheng, B. Zhang, C. Di, F. Li, C. Jin, W. Mi, L. Chen, W. Hu, *Angew. Chem. Int. Ed.* **2020**, *59*, 1118–1123; b) J. Dou, M. Q. Arguilla, Y. Luo, J. Li, W. Zhang, L. Sun, J. L. Mancuso, L. Yang, T. Chen, L. R. Parent, G. Skorupskii, N. J. Libretto, C. Sun, M. Yang, P. V. Dip, E. J. Brignole, J. T. Miller, J. Kong, C. H. Hendon, J. Sun, M. Dinca, *Nat. Mater.* **2021**, *20*, 222–228; c) H. Huang, Y. Zhao, Y. Bai, F. Li, Y. Zhang, Y. Chen, *Adv. Sci.* **2020**, *7*, 2000012; d) J. C. Bachman, J. S. Elias, C. J. Sun, Y. Shao-Horn, M. Dinca, *Nat. Mater.* **2017**, *16*, 220–224; e) H. T. B. Pham, J. Y. Choi, S. Huang, X. Wang, A. Claman, M. Stodolka, S. Yazdi, S. Sharma, W. Zhang, J. Park, *J. Am. Chem. Soc.* **2022**, *144*, 10615–10621; f) R. Iqbal, S. Ali, G. Yasin, S. Ibraheem, M. Tabish, M. Hamza, H. Chen, H. Xu, J. Zeng, W. Zhao, *Chem. Eng. J.* **2022**, *430*, 132642; g) D. Feng, T. Lei, M. M. R. Lukatskaya, J. Park, Z. Huang, M. Lee, L. Shaw, S. Chen, A. A. Yakovenko, A. Kulkarni, J. Xiao, K. Fredrickson, J. B. Tok, X. Zou, Y. Cui, Z. Bao, *Nat. Energy* **2018**, *3*, 30–36; h) J. Dou, L. Sun, Y. Ge, W. Li, C. H. Hendon, J. Li, S. Gul, J. Yano, E. A. Stach, M. Dinca, *J. Am. Chem. Soc.* **2017**, *139*, 13608–13611; i) Y. Lu, H. Zhong, J. Li, A. M. Dominic, Y. Hu, Z. Gao, Y. Jiao, M. Wu, H. Qi, C. Huang, L. J. Wayment, U. Kaiser, E. Spiecker, I. M. Weidinger, W. Zhang, X. Feng, R. Dong, *Angew. Chem. Int. Ed.* **2022**, *61*, e202208163; j) J. Park, M. Lee, D. Feng, Z. Huang, A. C. Hinckley, A. Yakovenko, X. Zou, Y. Cui, Z. Bao, *J. Am. Chem. Soc.* **2018**, *140*, 10315–10323; k) Y. Liu, S. Li, L. Dai, J. Li, J. Lv, Z. Zhu, A. Yin, P. Li, B. Wang, *Angew. Chem. Int. Ed.* **2021**, *60*, 16409–16415; l) J. Liu, D. Yang, Y. Zhou, G. Zhang, G. Xing, Y. Liu, Y. Ma, O. Terasaki, S. Yang, L. Chen, *Angew. Chem. Int. Ed.* **2021**, *60*, 14473–14479; m) Y. Lu, Y. Zhang, C. Y. Yang, S. Revuelta, H. Qi, C. Huang, W. Jin, Z. Li, V. Vega-Mayoral, Y. Liu, X. Huang, D. Pohl, M. Polozij, S. Zhou, E. Canovas, T. Heine, S. Fabiano, X. Feng, R. Dong, *Nat. Commun.* **2022**, *13*, 7240.  
 [9] a) A. Aykanat, Z. Meng, R. M. Stolz, C. T. Morrell, K. A. Mirica, *Angew. Chem. Int. Ed.* **2022**, *61*, e202113665; b) J. Yi, D. Si, R. Xie, Q. Yin, M. Zhang, Q. Wu, G. Chai, Y. Huang, R. Cao, *Angew. Chem. Int. Ed.* **2021**, *60*, 17108–17114; c) Z. Meng, J. Luo, W. Li, K. A. Mirica, *J. Am. Chem. Soc.* **2020**, *142*, 21656–21669; d) W. Li, L. Sun, J. Qi, P. Jarillo-Herrero, M. Dinca, J. Li, *Chem. Sci.* **2017**, *8*, 2859–2867; e) X. Qiu, H. Zhu, J. Huang, P. Liao, X. Chen, *J. Am. Chem. Soc.* **2021**, *143*, 7242–7246; f) H. Nagatomi, N. Yanai, T. Yamada, K. Shiraishi, N. Kimizuka, *Chem. Eur. J.* **2018**, *24*, 1806–1810; g) Z. Meng, A. Aykanat, K. A. Mirica, *J. Am. Chem. Soc.* **2019**, *141*, 2046–2053.  
 [10] R. Dong, Z. Zhang, D. C. Tranca, S. Zhou, M. Wang, P. Adler, Z. Liao, F. Liu, Y. Sun, W. Shi, Z. Zhang, E. Zschech, S. C. B. Mannsfeld, C. Felser, X. Feng, *Nat. Commun.* **2018**, *9*, 2637.  
 [11] a) A. Wu, W. Wang, H. Zhan, L. Cao, X. Ye, J. Zheng, P. Kumar, K. Chiranjeevulu, W. Deng, G. Wang, M. Yao, G. Xu, *Nano Res.* **2021**, *14*, 438–443; b) Y. Lin, W. Li, Y. Wen, G.

- Wang, X. Ye, G. Xu, *Angew. Chem. Int. Ed.* **2021**, *60*, 25758–25761; c) M. Yao, J. Xiu, Q. Huang, W. Li, W. Wu, A. Wu, L. Cao, W. Deng, G. Wang, G. Xu, *Angew. Chem. Int. Ed.* **2019**, *58*, 14915–14919; d) Y. Liu, M. Liu, S. Shang, W. Gao, X. Wang, J. Hong, C. Hua, Z. You, Y. Liu, J. Chen, *ACS Appl. Mater. Interfaces* **2023**, *15*, 16991–16998.
- [12] A. Salehi-Khojin, F. Khalili-Araghi, M. A. Kuroda, K. Y. Lin, J. P. Leburton, R. I. Masel, *ACS Nano* **2011**, *5*, 153–158.
- [13] E. Singh, M. Meyyappan, H. S. Nalwa, *ACS Appl. Mater. Interfaces* **2017**, *9*, 34544–34586.
- [14] R. Kumar, O. Al-Dossary, G. Kumar, A. Umar, *Nano-Micro Lett.* **2015**, *7*, 97–120.
- [15] a) R. K. Sharma, M. C. Bhatnagar, G. L. Sharma, *Sens. Actuators B* **1998**, *46*, 194–201; b) J. Lee, Y. Jung, S. H. Sung, G. Lee, J. Kim, J. Seong, Y. S. Shim, S. C. Jun, S. Jeon, *J. Mater. Chem. A* **2021**, *9*, 1159–1167.
- [16] a) M. Sun, S. Huang, L. Chen, Y. Li, X. Yang, Z. Yuan, B. Su, *Chem. Soc. Rev.* **2016**, *45*, 3479–3563; b) L. Sun, X. Liu, H. Zhou, *Chem. Soc. Rev.* **2015**, *44*, 5092–5147; c) C. Du, P. Li, Z. Zhuang, Z. Fang, S. He, L. Feng, W. Chen, *Coord. Chem. Rev.* **2022**, *466*, 214604.
- [17] a) H. Bahron, S. S. Khaidir, A. M. Tajuddin, K. Ramasamy, B. M. Yamin, *Polyhedron* **2019**, *161*, 84–92; b) V. Torabi, H. Kargar, A. Akbari, R. Behjatmanesh-Ardakani, H. Amiri Rudbari, M. Nawaz Tahir, *J. Coord. Chem.* **2018**, *71*, 3748–3762.
- [18] M. S. Yao, W. X. Tang, G. Wang, B. Nath, G. Xu, *Adv. Mater.* **2016**, *28*, 5229–5234.
- [19] a) R. Shen, X. Li, X. Xia, H. Liang, G. Wu, Y. Liu, C. Cheng, G. Du, *Chin. Sci. Bull.* **2012**, *57*, 2087–2093; b) G. Hou, Y. Xie, L. Wu, H. Cao, Y. Tang, G. Zheng, *Int. J. Hydrogen Energy* **2016**, *41*, 9295–9302; c) W. Li, X. Zhang, X. Guo, *Sens. Actuators B* **2017**, *244*, 509–521.
- [20] H. Jiang, L. Cao, Y. Li, W. Li, X. Ye, W. Deng, X. Jiang, G. Wang, G. Xu, *Chem. Commun.* **2020**, *56*, 5366–5369.

Manuscript received: May 4, 2023

Accepted manuscript online: June 6, 2023

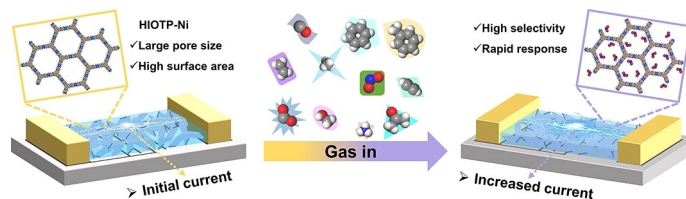
Version of record online: ■■■, ■■■

## Communications

## 2D MOFs

P. Chen, X. Su, C. Wang, G. Zhang,  
T. Zhang, G. Xu,\* L. Chen\* — e202306224

Two-Dimensional Conjugated Metal-Organic Frameworks with Large Pore Apertures and High Surface Areas for NO<sub>2</sub> Selective Chemiresistive Sensing



Two new two-dimensional conjugated metal-organic frameworks (2D *c*-MOFs) were synthesized via coordination of a new ligand (HAOTP) with metal ions (Ni<sup>2+</sup> and Cu<sup>2+</sup>). The resulting HIOTP-Ni MOF has a large pore aperture of

3.3 nm and a high surface area of 1300 m<sup>2</sup> g<sup>-1</sup>. As a result, it has exceptional performance as a chemiresistive sensor, with a highly selective (405%) and rapid response (1.69 min) towards 10 ppm NO<sub>2</sub> gas.



## SPACE RESERVED FOR IMAGE AND LINK

Share your work on social media! *Angewandte Chemie* has added Twitter as a means to promote your article. Twitter is an online microblogging service that enables its users to send and read short messages and media, known as tweets. Please check the pre-written tweet in the galley proofs for accuracy. If you, your team, or institution have a Twitter account, please include its handle @username. Please use hashtags only for the most important keywords, such as #catalysis, #nanoparticles, or #proteindesign. The ToC picture and a link to your article will be added automatically, so the **tweet text must not exceed 250 characters**. This tweet will be posted on the journal's Twitter account (follow us @angew\_chem) upon publication of your article in its final (possibly unpaginated) form. We recommend you to re-tweet it to alert more researchers about your publication, or to point it out to your institution's social media team.

Please check that the ORCID identifiers listed below are correct. We encourage all authors to provide an ORCID identifier for each coauthor. ORCID is a registry that provides researchers with a unique digital identifier. Some funding agencies recommend or even require the inclusion of ORCID IDs in all published articles, and authors should consult their funding agency guidelines for details. Registration is easy and free; for further information, see <http://orcid.org/>.

Pei Chen

Xi Su

Chuanzhe Wang

Dr. Guang Zhang

Dr. Ting Zhang

Prof. Gang Xu

Prof. Long Chen <http://orcid.org/0000-0001-5908-266X>